We are IntechOpen, the world's leading publisher of Open Access books Built by scientists, for scientists

6,900
Open access books available

186,000
International authors and editors

200M
Downloads

Our authors are among the

154
Countries delivered to

TOP 1%
most cited scientists

12.2%
Contributors from top 500 universities

WEB OF SCIENCE™

Selection of our books indexed in the Book Citation Index in Web of Science™ Core Collection (BKCI)

Interested in publishing with us?
Contact book.department@intechopen.com

Numbers displayed above are based on latest data collected.
For more information visit www.intechopen.com

7

Photoionization Cross Sections of Atomic Impurities in Spherical Quantum Dots

C. Y. Lin and Y. K. Ho
Institute of Atomic and Molecular Sciences, Academia Sinica
Taiwan

1. Introduction

With the advances of experimental techniques in fabrication and investigation of nano-scale structures, confined atomic systems become practical and useful models for the illustration of interesting phenomena arising from a system in dimensions comparable to the electronic de Broglie wavelength. The confined atomic models are widely used to study a variety of physical systems, such as impurities in quantum dots (Lin & Ho (2011)), atoms encapsulated in fullerenes (Connerade et al. (1999); Dolmatov et al. (2004)), and atoms under high pressure (de Groot & ten Seldam (1946); Michels et al. (1937)). In this article, we focus on the quantum confinement occurring in quantum dots. The emphasis is placed on the variation of electronic structures and photoionization properties of atomic impurities under the spatial confinement effect of quantum dots.

As a quantum confinement system, the quantum dot has attracted considerable attention due to not only its theoretical but also practical significance. In addition to the analogies of discrete structure in their optical and electrical features between a quantum dot and an atom, the coupled quantum dots provide a model to mimic molecules with tunable bonds (Alivisatos (1996); Schedelbeck et al. (1997)). On the other hand, the quantum dots also serve as contrast agents in bioimaging for biotechnological applications (Michalet et al. (2005)). It is well known that the quantum dot with atomic impurities is a suitable model for studying the semiconductor heterostructures. Recently, the enhancement of semiconductor nano-crystal performance due to the impurities has been reported in the literature (Cao (2011)), which indicates, for instance, that magnetic impurities can be doped to tune optical and magnetic properties.

The physical properties of confined atomic systems are greatly influenced by confinement potentials, which are unable to be determined through the direct measurement of experiment. Although *ab initio* calculations can comprehensively deal with the interaction in confined atomic systems, they may not provide a direct and simple physical interpretation. The usage of semi-empirical model potentials to mimic the interaction of confined atom and surrounding environment provides an efficient way to study the complex systems. The appropriate models, which might not treat the system comprehensively but take the important interaction into account, give a clear physical insight into complex problems. The confinement potentials associated with the structures of quantum dots are often modelled by the rectangular potential

well

$$V_{\mathrm{RECT}}(r) = \begin{cases} -V_0 & r \leq R; \\ 0 & r > R, \end{cases} \tag{1}$$

or the harmonic oscillator (parabolic) potential.

$$V_{\mathrm{HO}}(r) = -V_0 + \frac{V_0}{R^2} r^2, \tag{2}$$

where R determines the size of quantum dot, and V_0 gives the strength of confinement. The rectangular potential well has a simple but unrealistic form due to the non-parabolic shape at the center of quantum dots. Although the harmonic oscillator potential fulfils the parabolic property, the infinite depth and range of potential restrict the calculation of continuum states and fail to describe the charging of quantum dots with the finite number of electrons.

The Woods-Saxon potential given as

$$V_{\mathrm{WS}}(r) = \frac{V_0}{1 + \exp\left[(R - r)/\gamma\right]}, \tag{3}$$

where γ controls the slope of confinement potential, also has been used in the study of confined quantum system (Costa et al. (1999); Xie (2009)). It should be noted that the Woods-Saxon potential turns to be the rectangular potential well as $\gamma \to 0$. Another confinement potential flexible to model the different type of quantum dots is the so called power-exponential potential (Ciurla et al. (2002)),

$$V_{\mathrm{EP}}(r) = -V_0 \exp\left[-(r/R)^p\right]. \tag{4}$$

With the change of parameter p, the shape of potential is modified from the Gaussian potential $p = 2$ to the rectangular potential well $p = \infty$.

In this work, the systems of atomic impurities in spherical quantum dots characterized by finite oscillator (FO) and Gaussian potentials (Adamowski et al. (2000a;b); Kimani et al. (2008); Winkler (2004)) are investigated using the method of complex-coordinate rotation (Ho (1983); Reinhardt (1982)) in a finite-element discrete variable representation (FE DVR) (Balzer et al. (2010); Rescigno & McCurdy (2000)). The finite oscillator potential V_{FO} and Gaussian potential V_{G} are defined as

$$V_{\mathrm{FO}}(r) = -A\left(1 + \frac{B}{\sqrt{A}} r\right) \exp\left(-\frac{B}{\sqrt{A}} r\right) \tag{5}$$

and

$$V_{\mathrm{G}}(r) = -C \exp(-r^2/D^2), \tag{6}$$

where A and C are the confining strength of potentials, and the radii of dots are characterized inherently by $1/B$ and D for FO and Gaussian potentials, respectively. Figure 1 shows the examples of both potentials. The Gaussian potential being a special case of the power-exponential potential (Ciurla et al. (2002)) has a soft boundary of the potential. The one-electron energy spectrum for a Gaussian potential has been calculated by Adamowski et al. (Adamowski et al. (2000a;b)) using the variational method with Gaussian-type basis functions. The finite oscillator potentials as weakly confining potentials of quantum dots have been used to study the two-electron quantum dots by Winkler (Winkler (2004)), and

later applied to few-electron quantum dots (Kimani et al. (2008)). Both potentials have r^2-dependence near the center of quantum dots, which is the typical character of harmonic oscillators. It should be noted that the impurity is not taken into account for the quantum dots in above-mentioned investigations.

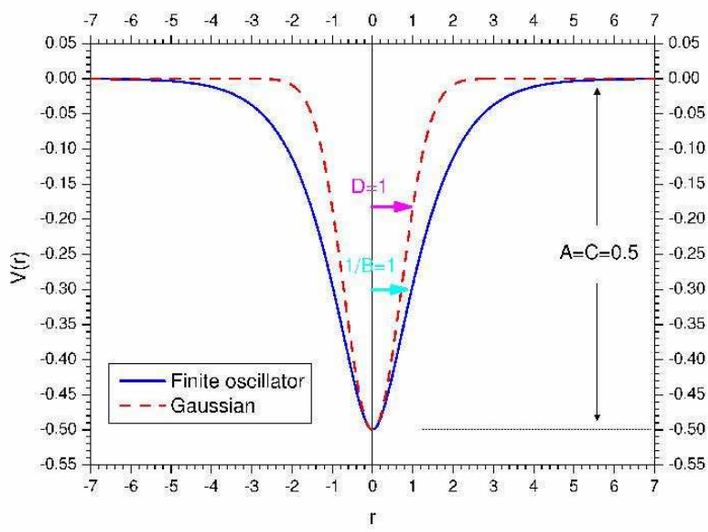

Fig. 1. Comparison of finite oscillator potential with Gaussian potential.

For the investigations of electronic structure and optical properties of atomic impurities in quantum dots, many efforts have been devoted to study hydrogenic impurity states in spherical quantum dots described by finite and infinite potential wells. The state energies of hydrogen impurity in spherical quantum dots with the infinite and finite well of rectangular potentials are explored by Chuu et al. (Chuu et al. (1992)), Yang et al. (Yang et al. (1998)), and Huang et al. (Huang et al. (1999)). Photoionization cross sections and oscillator strengths of hydrogenic impurities in spherical quantum dots are also obtained for the infinite and finite rectangular well models by Ham and Spector (Ham & Spector (n.d.)), Şahin (Şahin (2008)), and Stevanović (Stevanović (2010)). Recently, Lin and Ho (Lin & Ho (2011)) study the photoionization of hydrogen impurities in spherical quantum dots using the finite oscillator and Gaussian potentials. Chakraborty and Ho (Chakraborty & Ho (2011)) adopt the finite oscillator potential to describe the quantum dot for exploring the autoionization resonance states of helium impurities in quantum dots. In the present work, the alkali-metal atoms as impurities in the quantum dots are studied. On the basis of the finite oscillator and Gaussian models, the energy levels and photionization cross sections subject to the quantum confinement effect are illustrated.

The chapter is organized as follows. In Sec. 2, the FE DVR approach and complex-coordinate rotation method associated with the current work are described. The energy spectrum and photoionization cross sections varying with the different conditions of quantum dots for the lithium and sodium impurities are presented and discussed in Sec. 3. Section 4 summarizes this work and gives conclusions. Atomic units are used throughout unless otherwise noted.

2. Theoretical method

2.1 Finite-element discrete variable representation

The finite-element discrete variable representation (FE DVR) is a hybrid computation scheme taking advantage of the finite-element approach and the discrete variable representation to obtain the sparse kinetic-energy matrices and the diagonal representation of potential-energy matrices. Using this hybrid approach, the kinetic-energy matrix is block diagonal with matrix elements in compact expressions, and the potential-energy matrix elements are given by the potential values at grid points. This method has been implemented to investigate a variety of interesting physical problems, such as quantum-mechanical scattering problems (Rescigno & McCurdy (2000)), bright solitons in Bose-Einstein Condensates and ultracold plasmas (Collins et al. (2004)), non-equilibrium Greenąęs function calculations (Balzer et al. (2010)), and photoionization of impurities in quantum dots (Lin & Ho (2011)).

In the present work, the method of FE DVR which is detailed in references (Rescigno & McCurdy (2000)) and (Balzer et al. (2010)) is adopted to obtain the Hamiltonian matrix elements for atoms confined by quantum dots. Within the framework of FE DVR, the interval $[0,R_{max}]$ is divided into n_e finite elements, in which each element between $[x^i, x^{i+1}]$ is further subdivided by n_g Gauss quadrature points (see Fig. 2). Taking advantage of the standard Gauss-Lobatto points x_m and weights w_m (Michels (1963)), we define the generalized Gauss-Lobatto points,

$$x_m^i = \frac{1}{2}[(x^{i+1} - x^i)x_m + (x^{i+1} + x^i)], \tag{7}$$

and weights,

$$w_m^i = \frac{w_m}{2}(x^{i+1} - x^i). \tag{8}$$

It should be noted that $x_1^i = x^i$ and $x_{n_g}^i = x^{i+1}$ because $x_1 = -1$ and $x_{n_g} = 1$. In calculations, the integrals are approximated by Gauss-Lobatto quadrature,

$$\int_{x^i}^{x^{i+1}} \psi(r)dr \simeq \psi(x^i)w_1^i + \sum_{m=2}^{n_g-1} \psi(x_m^i)w_m^i + \psi(x^{i+1})w_{n_g}^i. \tag{9}$$

The wave functions are expanded in terms of local basis functions (see Fig. 2),

$$\chi_m^i(x) = \begin{cases} \dfrac{[f_{n_g}^i(x) + f_1^{i+1}(x)]}{\sqrt{(w_{n_g}^i + w_1^{i+1})}} & \text{for m=1 (bridge);} \\ \dfrac{f_m^i(x)}{\sqrt{w_m^i}} & \text{for else (element),} \end{cases} \tag{10}$$

where the Lagrange interpolating polynomials or so-called Lobatto shape functions $f_m^i(x)$ are given as

$$f_m^i(x) = \begin{cases} \prod\limits_{m' \neq m} \dfrac{(x - x_{m'}^i)}{(x_m^i - x_{m'}^i)} & \text{for } x^i \leq x \leq x^{i+1}; \\ 0 & \text{for } x < x^i \text{ or } x > x^{i+1}. \end{cases} \tag{11}$$

The bridge basis function $\chi_1^i(x)$ in Eq. (10) is in charge of connecting the adjacent elements to ensure the continuity of wave functions at end points of each finite element.

Based on the properties of the Lobatto shape functions and the approximation of Gauss-Lobatto quadrature for integrals, the matrix elements of kinetic-energy operator, $T = -\frac{1}{2}\frac{\mathrm{d}^2}{\mathrm{d}x^2}$, in FE DVR are evaluated by analytic formulas,

$$T^{i_1,i_2}_{m_1,m_2} = \langle \chi^{i_1}_{m_1}|T|\chi^{i_2}_{m_2}\rangle = \frac{1}{2}(\delta_{i_1,i_2}+\delta_{i_1,i_2\pm1})\int_0^\infty \mathrm{d}x \frac{\mathrm{d}}{\mathrm{d}x}\chi^{i_1}_{m_1}(x)\frac{\mathrm{d}}{\mathrm{d}x}\chi^{i_2}_{m_2}(x)$$

$$= \begin{cases} \frac{1}{2}\dfrac{\delta_{i_1,i_2}\tilde{T}^{i_1}_{m_1,m_2}}{\sqrt{w^{i_1}_{m_1}w^{i_2}_{m_2}}} & (m_1>1,\, m_2>1); \\ \frac{1}{2}\dfrac{(\delta_{i_1,i_2}\tilde{T}^{i_1}_{n_g,m_2}+\delta_{i_1,i_2-1}\tilde{T}^{i_2}_{1,m_2})}{\sqrt{w^{i_2}_{m_2}(w^{i_1}_{n_g}+w^{i_1+1}_1)}} & (m_1=1,\, m_2>1); \\ \frac{1}{2}\dfrac{(\delta_{i_1,i_2}\tilde{T}^{i_1}_{m_1,n_g}+\delta_{i_1,i_2+1}\tilde{T}^{i_1}_{m_1,1})}{\sqrt{w^{i_1}_{m_1}(w^{i_2}_{n_g}+w^{i_2+1}_1)}} & (m_1>1,\, m_2=1); \\ \frac{1}{2}\dfrac{(\delta_{i_1,i_2}(\tilde{T}^{i_1}_{n_g,n_g}+\tilde{T}^{i_1+1}_{1,1})+\delta_{i_1,i_2-1}\tilde{T}^{i_2}_{1,n_g}+\delta_{i_1,i_2+1}\tilde{T}^{i_1}_{n_g,1})}{\sqrt{(w^{i_1}_{n_g}+w^{i_1+1}_1)(w^{i_2}_{n_g}+w^{i_2+1}_1)}} & (m_1=m_2=1), \end{cases} \tag{12}$$

in which the term $\tilde{T}^i_{m_1,m_2}$ is defined as

$$\tilde{T}^i_{m_1,m_2} = \sum_m \frac{\mathrm{d}f^i_{m_1}(x^i_m)}{\mathrm{d}x}\frac{\mathrm{d}f^i_{m_2}(x^i_m)}{\mathrm{d}x}w^i_m. \tag{13}$$

According to Eq. (11), the first derivatives of the Lobatto shape functions at the quadrature points are given as

$$\frac{df^i_{m_1}(x^i_m)}{dx} = \begin{cases} \dfrac{1}{(x^i_{m_1}-x^i_m)}\displaystyle\prod_{m'\neq m_1,m}\frac{(x^i_m-x^i_{m'})}{(x^i_{m_1}-x^i_{m'})} & \text{for } m_1\neq m; \\ \frac{1}{2w^i_{m_1}}(\delta_{m_1,n_g}-\delta_{m_1,1}) & \text{for } m_1=m. \end{cases} \tag{14}$$

The matrix of the local potential-energy operator $V(x)$ in FE DVR has a diagonal representation with matrix element values equal to potential values at grid points, i.e.,

$$V^{i_1,i_2}_{m_1,m_2} = \int_0^\infty \mathrm{d}x\chi^{i_1}_{m_1}(x)V(x)\chi^{i_2}_{m_2}(x) = \delta_{i_1,i_2}\delta_{m_1,m_2}\tilde{V}^{i_1}_{m_1}, \tag{15}$$

with

$$\tilde{V}^i_m = \begin{cases} V(x^i_m) & \text{for } m>1; \\ \dfrac{V(x^i_{n_g})w^i_{n_g}+V(x^{i+1}_1)w^{i+1}_1}{w^i_{n_g}+w^{i+1}_1} & \text{for } m=1. \end{cases} \tag{16}$$

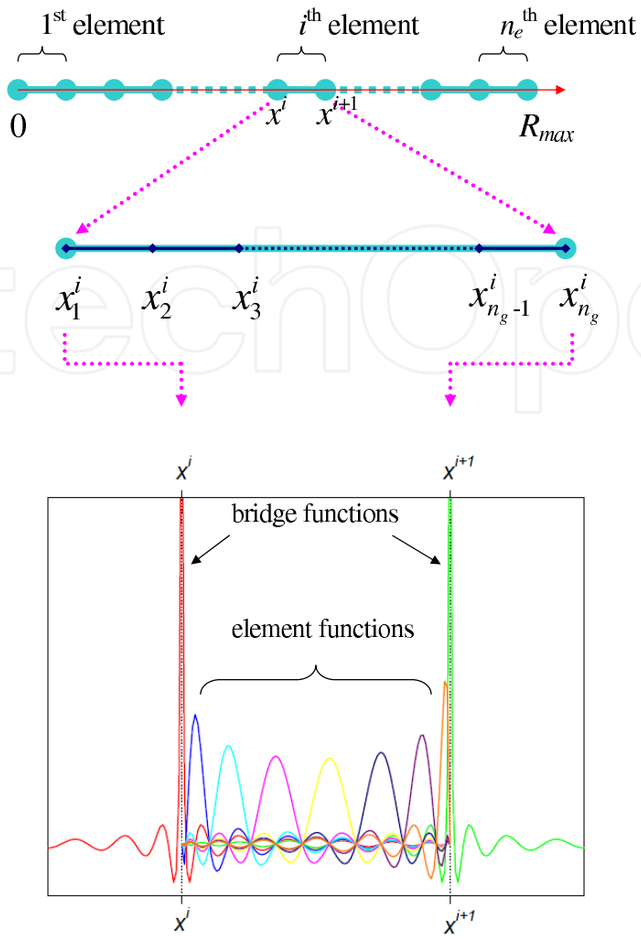

Fig. 2. Interval between 0 and R_{max} divided into n_e finite elements with n_g Gauss quadrature points and selected local basis functions (bridge and element functions) distributed in each finite element.

2.2 The method of complex coordinate rotation

The radial Schrödinger equation for the atomic impurity in spherical quantum dots is given as

$$\left[-\frac{1}{2}\frac{\mathrm{d}^2}{\mathrm{d}r^2}+V(r)\right]\phi(r)=E\phi(r), \tag{17}$$

where $V(r)$ is defined as

$$V(r)=\frac{l(l+1)}{2r^2}+U_a(r)+V_{\mathrm{QD}}(r), \tag{18}$$

where U_a is the atomic potential, and V_{QD} is given by V_{FO} for the confinement of finite oscillator potential (see equation (5)) or V_{G} for the Gaussian potential (see equation (6)). Within the framework of the complex scaling approach, the real coordinate r is transformed to complex coordinate z by the mapping

$$z=r\mathrm{e}^{\mathrm{i}\Theta}, \tag{19}$$

which turns the generalized Gauss-Lobatto points and weights in Eqs. (7) and (8) to be complex, i.e.,

$$x_m^i \to x_m^i e^{i\Theta}, \tag{20}$$

and

$$w_m^i \to w_m^i e^{i\Theta}. \tag{21}$$

The integrations of kinetic- and potential-energy matrix elements are performed along the complex path instead of the real axis. It turns out that the calculations of Eqs. (12) and (16) by the complex quadrature points and weights are equivalent to the usage of the real points and weights with the complex scaled operators. In other words, to obtain the complex scaled matrix elements, we can perform the transformation of the operators in advance,

$$-\frac{1}{2}\frac{d^2}{dr^2} \to -\frac{e^{-2i\Theta}}{2}\frac{d^2}{dr^2} \tag{22}$$

and

$$V(r) \to V(re^{i\Theta}), \tag{23}$$

followed by the implementation of integrals in real quadrature points and weights.

Through the standard diagonalization procedure, complex eigenvalues and eigenvectors are obtained. In the dipole approximation, the photoionization cross sections can be obtained by the optical theorem

$$\sigma(\omega) = \frac{4\pi\omega}{c}\mathrm{Im}(\alpha^-(\omega)), \tag{24}$$

where ω is the photon energy and c is the speed of light, i.e., the inverse fine-structure constant. The negative frequency component of the polarizability $\alpha^-(\omega)$ (Buchleitner et al. (1994); Rescigno & McKoy (1975)) calculated along the complex path C is given as

$$\alpha^-(\omega) = \int d\vartheta \int d\varphi \int_C dz\, z^2 \psi_0^\dagger(z,\vartheta,\varphi)\mu(z,\vartheta,\varphi)\psi^-(z,\vartheta,\varphi), \tag{25}$$

where μ is the component of the dipole operator along the direction of light polarization. The initial wave function ψ_0 with energy E_0 and the final scattered wave function ψ^- fulfill the equation

$$[H(z,\vartheta,\varphi) - E_0 - \omega]\,\psi^-(z,\vartheta,\varphi) = \mu(z,\vartheta,\varphi)\psi_0(z,\vartheta,\varphi). \tag{26}$$

3. Results and discussion

3.1 Lithium impurities in quantum dots

The method of complex coordinate rotation combined with the FE DVR approach are applied to investigate the state energies and photoionization cross sections of lithium impurities in the spherical quantum dots. The model potentials (Schweizer et al. (1999)), which are given as

$$U_a(r) = -\frac{1}{r}\left[\tilde{Z} + (Z - \tilde{Z}\exp(-a_1 r) + a_2 r\exp(-a_3 r))\right], \tag{27}$$

are adopted to simulate the alkali metals for the interaction of multi-electron core with the single valence electron. The parameters a_i $(i = 1,2,3)$ of model potentials optimized by a least-square fit to experimental energies are listed in Table 1 for the lithium and sodium atoms. The energies of ground and first few excited states obtained by this model potential

for the lithium atom are compared to the experimental data (Ralchenko et al. (2011)) in Table 2. Although the calculated ground-state energy of lithium atom is not as precise as the energy of excited states, the photoionization cross sections of free lithium atom as shown in Table 3 are in good agreement with other theoretical predictions.

Atom	$\bar{Z}$	Z	a_1	a_2	a_3
Li	1	3	3.395	3.212	3.207
Na	1	11	7.902	23.51	2.688

Table 1. Parameters of model potentials for lithium and sodium atoms.

	Theory		Experiment
	Present work	Sahoo & Ho	NIST
$1s^2 2s$	-0.197331	-0.198141	-0.198142
$1s^2 2p$	-0.130068		-0.130235
$1s^2 3s$	-0.074123		-0.074182
$1s^2 3p$	-0.057232		-0.057236

Table 2. Energies of ground and excited states for lithium model potential are compared with experimental values. Results of Sahoo & Ho refer to (Sahoo & Ho (2006)). Experimental data by NIST refer to (Ralchenko et al. (2011)).

ϵ	Present results	Sahoo & Ho	Peach et al.
0.01	1.568	1.470	1.565
0.03	1.638	1.551	1.640
0.05	1.653	1.575	1.659
0.10	1.557	1.500	1.571
0.50	0.568	0.562	0.580
1.00	0.218	0.217	0.218

Table 3. Photoionization cross sections (in units of Mb) of free lithium atom as functions of photoelectron energies ϵ (in atomic units). Results of Sahoo & Ho refer to (Sahoo & Ho (2006)). Data by Peach et al. refer to (Peach et al. (1988)).

In the present work, the energy levels of lithium impurities with the principal quantum number $n = 2$–3 and angular momentum quantum number $l = 0$–1 for the valence electron are calculated for the quantum dots modelled by the FO and Gaussian potentials. In Fig. 3, the $1s^2 2s$ and $1s^2 3s$ state energies of lithium impurities varying with the dot radii, $1/B$ and D for the FO and Gaussian potential, respectively, from 10^{-1} to 10^3 a.u. are displayed for the several confining strengths of potentials, A and C. Since the cases of $1/B = D = 0$ correspond to the free lithium atoms, the levels belonging to different confining strengths merge into one of the free lithium levels as the dot radii approach zero. With increasing the dot radii, the level energies are decreased until reaching a limit, which is equal to the energy of free lithium atom combined with the confining strength of potential, A or C. In other words, the total energy is then shifted down by an amount of A or C for the FO and Gaussian potentials, respectively. As long as the dot radii are small such that the confinement effect is negligible, the level energies are close to the energies of free atoms. The increased dot radii leading to the stronger confinement of quantum dots cause the wave function trapped into the inner region of a deeper potential well. As a result, the corresponding energies are decreased. For a specific confining strength of potential, $A = C = 0.5$ a.u., the energy variations of levels $1s^2 2s$, $1s^2 2p$, $1s^2 3s$, and $1s^2 3p$ with quantum dot radii ranging from 10^{-1} to 10^3 a.u. are shown in Fig. 4.

The rapidly downward shifts in $1s^2np$ levels caused by the confinement effect have analogy to the $1s^2ns$ levels.

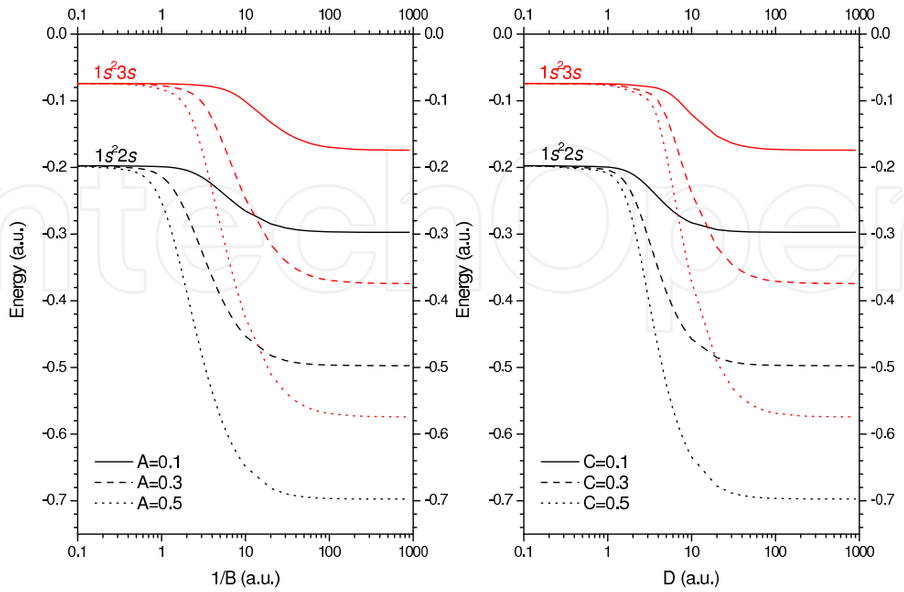

(a) Finite oscillator model (b) Gaussian model

Fig. 3. Energies of $1s^22s$ and $1s^23s$ states as functions of quantum dot radii ($1/B$ or D in atomic units) for several confining strengths of potentials (A or C in atomic units).

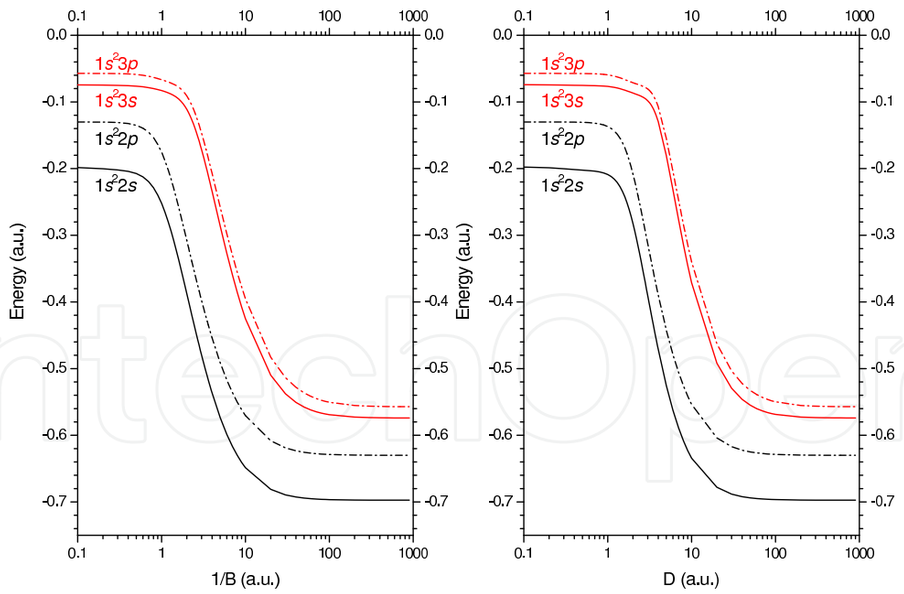

(a) Finite oscillator model (b) Gaussian model

Fig. 4. State energies of $1s^2nl$ ($n = 2$–3 and $l = 0$–1) as functions of quantum dot radii ($1/B$ or D) for the confining strengths of potentials $A = C = 0.5$ a.u.

The influence of quantum dot size on the photoionization cross sections of ground-state lithium impurities is demonstrated in Fig. 5 for the FO and Gaussian potentials with the

confining strengths of potentials $A = C = 0.5$. The cross sections varying with the selected radii of quantum dots show the drastic change for photon energies near the ionization threshold. As observed in Fig. 5 for the both models of quantum dots, the cross sections of $1/B = D = 0.3$ are close to the data of the free lithium case ($1/B = D = 0$) for high photoelectron energies, but reduced for low photonelectron energies. With increasing the size of quantum dot, the cross sections are gradually enhanced, and reach maximum values at $1/B \sim 1.5$ and $D \sim 3.0$ for the FO and Gaussian model, respectively. As the dot radius is further increased, the cross sections are deceased from the maximum values gradually.

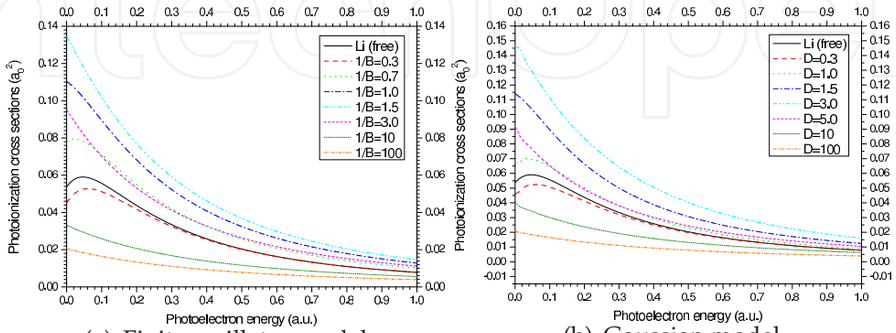

(a) Finite oscillator model (b) Gaussian model

Fig. 5. Photoionization cross sections as functions of photoelectron energies for several radii ($1/B$ and D in atomic units) of quantum dots with confining strengths of potentials $A = C = 0.5$.

One of striking properties due to the quantum confinement effect is the appearance of resonance-like profile in the photoionization cross sections as functions of quantum dot radii for a given photon energy. In Figs. 6, the cross sections as functions of confining strengths A and dot radii $1/B$ of the FO potentials are displayed for photon energies $\omega = 1$ and 3 a.u., respectively. For a given A, the occurrence of resonance-like structure demonstrates the constructive interference between the ground and continuum states due to the wave functions altered by the confinement effect of quantum dots. It is noticed that the peak of resonance-like profile rises with increasing the confining strength of potential. For the Gaussian potentials, the photoionization cross sections as functions of confining strengths C and dot radii D are shown in Fig. 7. The variation of cross sections with the confining strengths of potentials and dot radii resembles the results of the FO potentials, and the resonance-like profile of cross sections is also revealed. The numerical data of photoionization cross sections varying with the photoelectron energies are listed in Tables 4 and 5 for the FO and Gaussian potentials, respectively.

3.2 Sodium impurities in quantum dots

To investigate the state energies and photoionization cross sections of sodium impurities in the spherical quantum dots, we utilize the model potential in Eq. (27) with parameters given in Table 1 to describe the interaction of multi-electron core with the single valence electron for the sodium atom. The energies of ground and first few excited states calculated by this model potential for the sodium atom are compared to the experimental data (Ralchenko et al. (2011)) in Table 6.

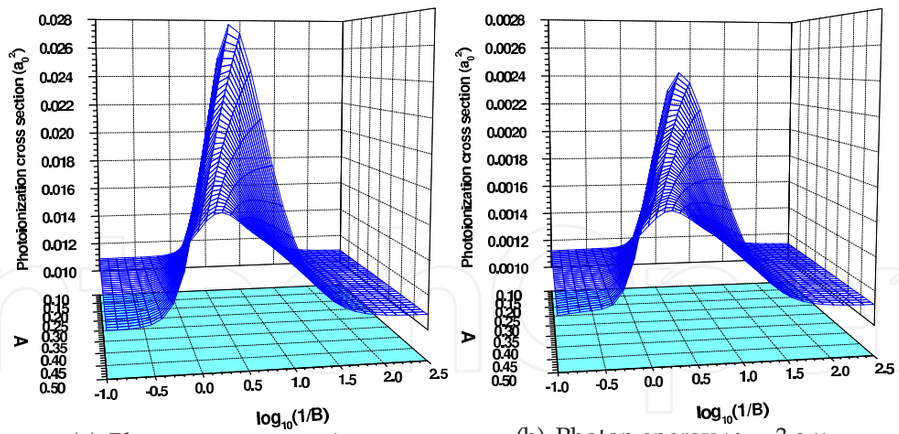

(a) Photon energy $\omega = 1$ a.u. (b) Photon energy $\omega = 3$ a.u.

Fig. 6. Photoionization cross sections as functions of confining strengths (A in atomic units) and quantum dot radii ($1/B$ in atomic units) for finite oscillator potentials.

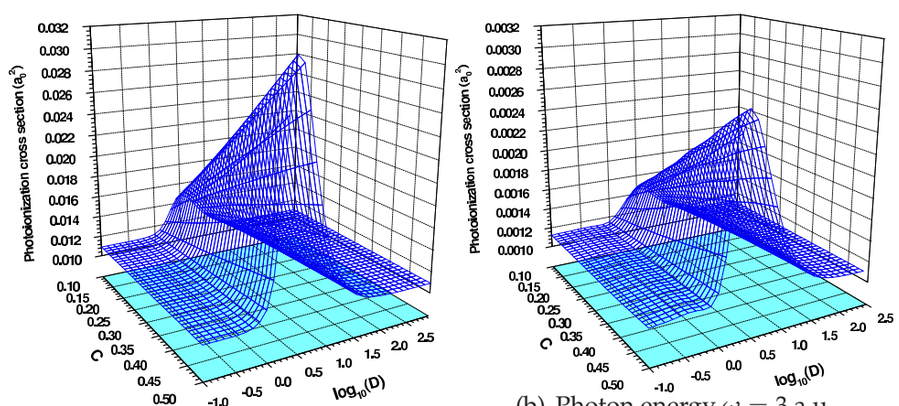

(a) Photon energy $\omega = 1$ a.u. (b) Photon energy $\omega = 3$ a.u.

Fig. 7. Photoionization cross sections as functions of confining strengths (C in atomic units) and quantum dot radii (D in atomic units) for Gaussian potentials.

In Fig. 8, the energies of levels $2p^6 3s$ and $2p^6 4s$ of sodium impurities varying with the dot radii, $1/B$ and D for the FO and Gaussian potential, respectively, in between 10^{-1} and 10^3 a.u. are presented for the several confining strengths of potentials, A and C. The levels associated with different confining strengths of potentials merge into one of the free sodium levels for the dot radii approaching zero. On the contrary, the level energies split to different energy limits corresponding to the combined energy of free sodium atom with the confining strengths of potential as the radius of quantum dot is large. For a specific confining strength of potential, $A = C = 0.5$ a.u., the energy variations of levels $2p^6 3s$, $2p^6 3p$, $2p^6 4s$, and $2p^6 4p$ with quantum dot radii ranging from 10^{-1} to 10^3 a.u. are shown in Fig. 9.

In Fig. 10, the photoionization cross sections of ground-state sodium impurities in spherical quantum dots characterized by the FO and Gaussian models of confining strengths $A = C = 0.5$ are presented. The variation of cross sections with selected radii of quantum dots shows the influence of quantum confinement on the photoionization. As observed in Fig. 10 for the both model potentials with small parameters $1/B$ and D, the photoionization cross sections

ω_p	$1/B = 0.8$	$1/B = 3.0$	$1/B = 5.0$	$1/B = 10$
0.2	4.79447(-2)	6.26482(-2)	4.75992(-2)	3.13920(-2)
0.4	2.84476(-2)	3.70083(-2)	2.85878(-2)	1.96808(-2)
0.6	1.80247(-2)	2.36864(-2)	1.86717(-2)	1.32830(-2)
0.8	1.21964(-2)	1.61640(-2)	1.29792(-2)	9.46338(-3)
1.0	8.68848(-3)	1.15891(-2)	9.45430(-3)	7.02362(-3)
1.5	4.35280(-3)	5.87191(-3)	4.93428(-3)	3.78125(-3)
2.0	2.52575(-3)	3.43660(-3)	2.94528(-3)	2.29925(-3)
2.5	1.60966(-3)	2.20681(-3)	1.91726(-3)	1.51494(-3)
3.0	1.09482(-3)	1.51144(-3)	1.32609(-3)	1.05669(-3)
3.5	7.81176(-4)	1.08537(-3)	9.59280(-4)	7.69130(-4)
4.0	5.78273(-4)	8.08194(-4)	7.18347(-4)	5.78660(-4)

Table 4. Photoionization cross sections (in a_0^2) as functions of photoelectron energies ω_p (in atomic units) for finite oscillator potentials of $A = 0.3$ a.u. and $1/B = 0.8$, 3.0, 5.0 and 10 a.u. $a(b)$ denotes $a \times 10^b$.

ω_p	$D = 0.8$	$D = 3.0$	$D = 5.0$	$D = 10$
0.2	4.41468(-2)	7.40039(-2)	5.46382(-2)	3.12982(-2)
0.4	2.64195(-2)	4.42053(-2)	3.21495(-2)	1.96037(-2)
0.6	1.67271(-2)	2.81879(-2)	2.06879(-2)	1.32432(-2)
0.8	1.12819(-2)	1.90666(-2)	1.42416(-2)	9.44659(-3)
1.0	8.00689(-3)	1.35329(-2)	1.03097(-2)	7.01908(-3)
1.5	3.97977(-3)	6.70843(-3)	5.34077(-3)	3.78682(-3)
2.0	2.29879(-3)	3.87066(-3)	3.17933(-3)	2.30576(-3)
2.5	1.46226(-3)	2.46429(-3)	2.06729(-3)	1.52060(-3)
3.0	9.94378(-4)	1.67902(-3)	1.42909(-3)	1.06132(-3)
3.5	7.10053(-4)	1.20178(-3)	1.03348(-3)	7.72856(-4)
4.0	5.26265(-4)	8.92958(-4)	7.73777(-4)	5.81669(-4)

Table 5. Photoionization cross sections (in a_0^2) as functions of photoelectron energies ω_p (in atomic units) for Gaussian potentials of $C = 0.3$ a.u. and $D = 0.8$, 3.0, 5.0 and 10 a.u. $a(b)$ denotes $a \times 10^b$.

	Theory		Experiment
	Present work	Sahoo & Ho	NIST
$2p^6 3s$	-0.188860	-0.188857	-0.188858
$2p^6 3p$	-0.111520		-0.111600
$2p^6 4s$	-0.071672		-0.071578
$2p^6 4p$	-0.050985		-0.050934

Table 6. Energies of ground and excited states for sodium model potential are compared with experimental values. Results of Sahoo & Ho refer to (Sahoo & Ho (2006)). Experimental data by NIST refer to (Ralchenko et al. (2011)).

slightly deviate from the data of the free sodium case ($1/B = D = 0$). With increasing the size of quantum dots, the humps of cross sections are enlarged. For $1/B$ and D larger than

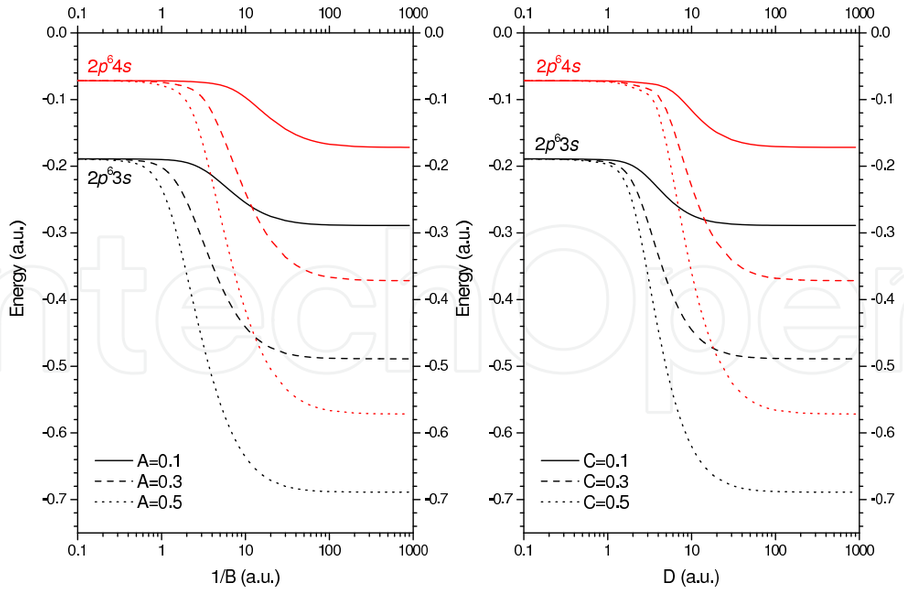

(a) Finite oscillator model (b) Gaussian model

Fig. 8. Energies of $2p^6 3s$ and $2p^6 4s$ states as functions of quantum dot radii ($1/B$ or D in atomic units) for several confining strengths of potentials (A or C in atomic units).

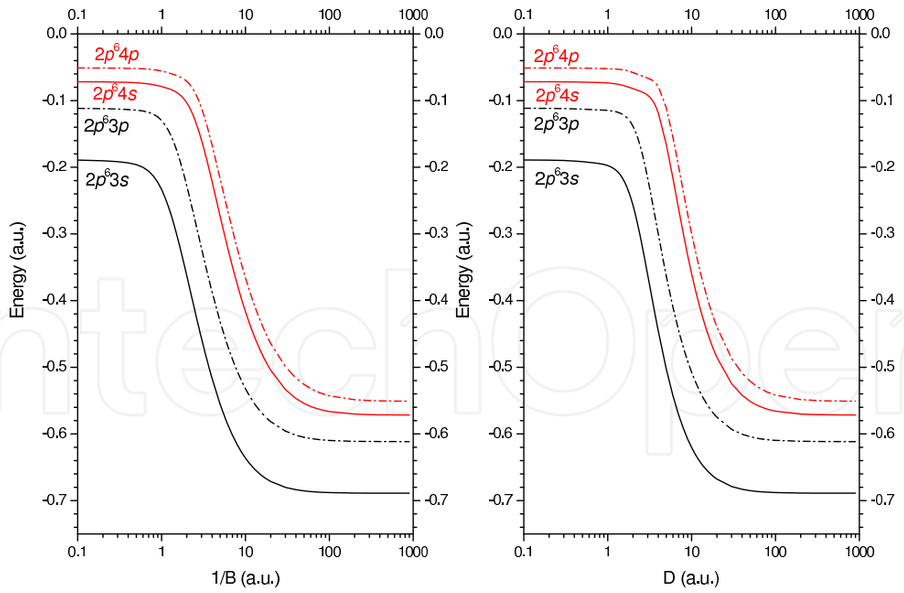

(a) Finite oscillator model (b) Gaussian model

Fig. 9. State energies of $2p^6 nl$ ($n = 3$–4 and $l = 0$–1) as functions of quantum dot radii ($1/B$ or D) for the confining strengths of potentials $A = C = 0.5$ a.u.

5, the hump disappears and cross sections are reduced with the further increase of quantum dot radii. The existence of a Cooper minimum in the photoionization cross sections of free sodium atoms is well known (Cooper (1962); Marr & Creek (1968)). It is particular interesting to notice that the Cooper minimum is shifted back and forth and vanished eventually from the threshold energy with the change of quantum dot size.

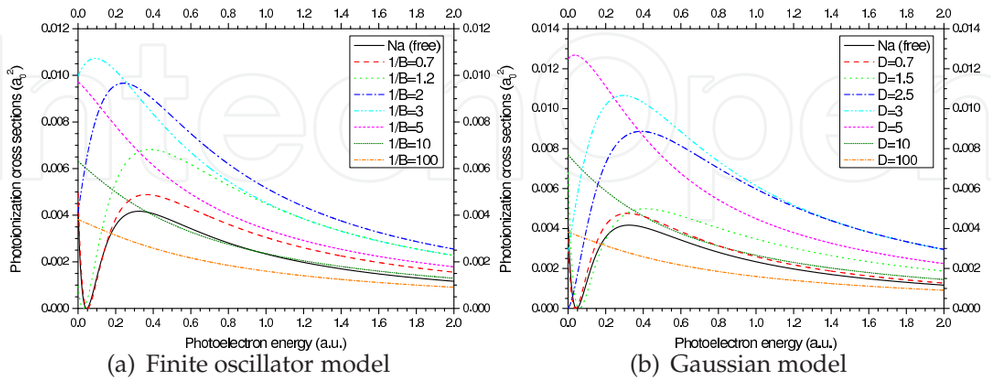

(a) Finite oscillator model (b) Gaussian model

Fig. 10. Photoionization cross sections as functions of photoelectron energies for several radii ($1/B$ and D in atomic units) of quantum dots with confining strengths $A = C = 0.5$.

Although the photoionization cross sections vary enormously and intricately with the size of quantum dots for photon energies near the threshold energy, the cross sections exhibit regular variation and resonance-like behavior for higher photon energies. In Figs. 11, the cross sections as functions of confining strengths A and dot radii $1/B$ of the FO potentials are displayed for photon energies $\omega = 1$ and 3 a.u., respectively. For a given confining strength of potential A, the resonance-like profile can be seen for photoionization cross sections varying with the dot radii $1/B$. The positions of resonance peak are shifted with the change of confining strength A. Because the photoionization cross sections are increased monotonically

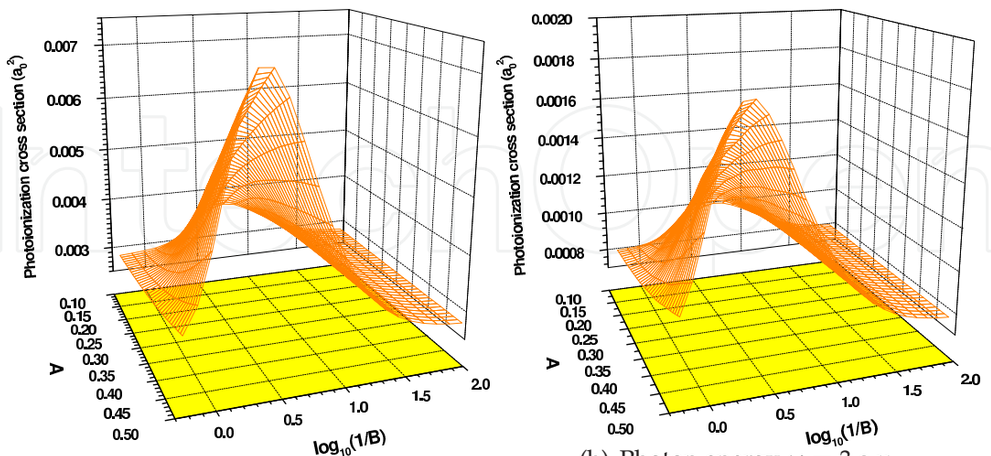

(a) Photon energy $\omega = 1$ a.u. (b) Photon energy $\omega = 3$ a.u.

Fig. 11. Photoionization cross sections as functions of confining strengths (A in atomic units) and quantum dot radii ($1/B$ in atomic units) for finite oscillator potentials.

with increasing the confining strength A for a given dot radius $1/B$, the peak of resonance rises with increasing the confining strengths of potentials.

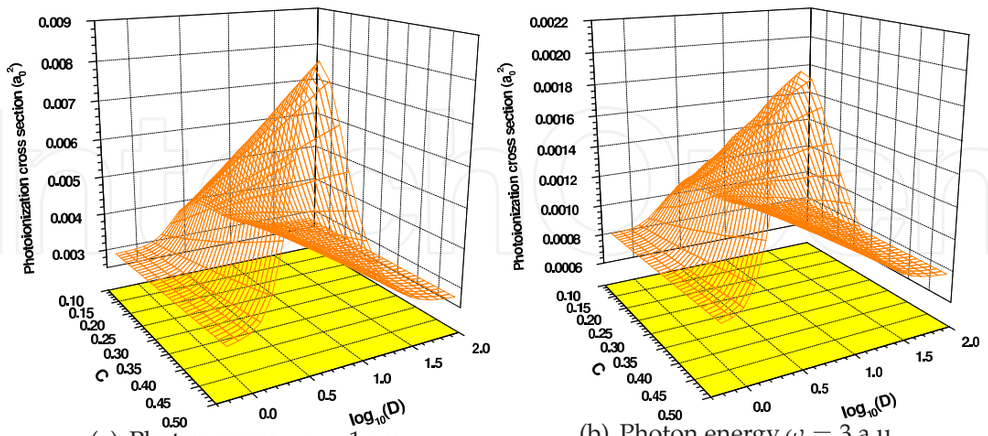

(a) Photon energy $\omega = 1$ a.u. (b) Photon energy $\omega = 3$ a.u.

Fig. 12. Photoionization cross sections as functions of confining strengths (C in atomic units) and quantum dot radii (D in atomic units) for Gaussian potentials.

For the Gaussian model, the photoionization cross sections as functions of confining strengths C and dot radii D are shown in Fig. 12. The variation of cross sections with the confining strengths of potentials and dot radii resembles the results of the FO potentials, and the resonance-like profile of cross sections is also revealed. To make the comparisons of FO model to the Gaussian model for the identical confining strengths $A = C$, the numerical data of photoionization cross sections varying with the photoelectron energies are listed in Tables 7 and 8 for the selected radii of quantum dots.

ω_p	$1/B = 0.8$	$1/B = 3.0$	$1/B = 5.0$	$1/B = 10$
0.2	3.74494(-3)	7.64326(-3)	7.91640(-3)	5.90620(-3)
0.4	4.44278(-3)	7.25065(-3)	6.51128(-3)	4.71764(-3)
0.6	3.81066(-3)	5.99769(-3)	5.19782(-3)	3.79446(-3)
0.8	3.15905(-3)	4.91032(-3)	4.21919(-3)	3.12203(-3)
1.0	2.64072(-3)	4.07371(-3)	3.50190(-3)	2.62573(-3)
1.5	1.80224(-3)	2.74326(-3)	2.38394(-3)	1.83387(-3)
2.0	1.32701(-3)	2.00153(-3)	1.75935(-3)	1.37624(-3)
2.5	1.02749(-3)	1.54056(-3)	1.36656(-3)	1.08106(-3)
3.0	8.23278(-4)	1.22982(-3)	1.09860(-3)	8.75958(-4)
3.5	6.76071(-4)	1.00775(-3)	9.05143(-4)	7.25869(-4)
4.0	5.65586(-4)	8.42125(-4)	7.59630(-4)	6.11833(-4)

Table 7. Photoionization cross sections (in a_0^2) as functions of photoelectron energies ω_p (in atomic units) for finite oscillator potentials of $A = 0.3$ a.u. and $1/B = 0.8$, 3.0, 5.0 and 10 a.u. $a(b)$ denotes $a \times 10^b$.

ω_p	$D = 0.8$	$D = 3.0$	$D = 5.0$	$D = 10$
0.2	3.93638(-3)	6.91812(-3)	9.30767(-3)	6.05882(-3)
0.4	4.41554(-3)	7.77475(-3)	7.57303(-3)	4.77588(-3)
0.6	3.70173(-3)	6.76452(-3)	5.94424(-3)	3.82507(-3)
0.8	3.02736(-3)	5.63360(-3)	4.75905(-3)	3.14297(-3)
1.0	2.50772(-3)	4.69180(-3)	3.91035(-3)	2.64251(-3)
1.5	1.68942(-3)	3.13333(-3)	2.62412(-3)	1.84642(-3)
2.0	1.23644(-3)	2.25964(-3)	1.92403(-3)	1.38660(-3)
2.5	9.54678(-4)	1.72367(-3)	1.48954(-3)	1.08981(-3)
3.0	7.64071(-4)	1.36737(-3)	1.19525(-3)	8.83429(-4)
3.5	6.27312(-4)	1.11558(-3)	9.83654(-4)	7.32305(-4)
4.0	5.24941(-4)	9.29355(-4)	8.24908(-4)	6.17421(-4)

Table 8. Photoionization cross sections (in a_0^2) as functions of photoelectron energies ω_p (in atomic units) for Gaussian potentials of $C = 0.3$ a.u. and $D = 0.8$, 3.0, 5.0 and 10 a.u. $a(b)$ denotes $a \times 10^b$.

4. Conclusions

The lithium and sodium impurities in spherical quantum dots are investigated using the method of complex-coordinate rotation in the finite-element discrete variable representation. Utilizing the FO and Gaussian potentials to mimic the environment of quantum dots, we study the energy spectra and photoionization of alkali metal impurities under the influence of quantum confinement effect. The level energies of impurities in the quantum dots are calculated for the both FO and Gaussian potentials in a variety of dot radii and confining strengths of potentials. The downward shift of impurity energy toward the combined energy of the free atom and the amplitude of the confining strength of potential is exhibited. The quantum confinement effect on the impurity energies due to the FO model is compared to the Gaussian model. The photoionization cross sections as functions of photoelectron energies are presented for the selected dot radii. The sensitivity of cross sections near the threshold energies to the dot radii demonstrates the significance of quantum confinement effect on the photoionization. The photoionization cross sections varying with different dot radii and confining strengths of potentials are given for specific photon energies. The enhancement of the constructive interference between the ground and continuum states due to the quantum confinement leads to the resonance-like profile for the cross sections varying with the dot radii at a given photon energy. The positions of resonance peak are associated with the confining strength. It is noted that the Cooper minimum existing in the photoionization cross sections of sodium impurities is shifted back and forth in energy positions and vanished eventually from the threshold because of the effect of quantum confinement.

This work is financially supported by the National Science Council of Taiwan.

5. References

Adamowski, J., Sobkowicz, M., Szafran, B. & Bednarek, S. (2000a). Electron pair in a gaussian confining potential, *Physical Review B* 62: 4234–4237.

Adamowski, J., Sobkowicz, M., Szafran, B. & Bednarek, S. (2000b). Erratum: Electron pair in a gaussian confining potential [phys. rev. b **62** , 4234 (2000)], *Physical Review B* 62: 13233–13233.

Alivisatos, A. P. (1996). Semiconductor clusters, nanocrystals, and quantum dots, *Science* 271: 933–937.

Balzer, K., Bauch, S. & Bonitz, M. (2010). Efficient grid-based method in nonequilibrium Green's function calculations: Application to model atoms and molecules, *Physical Review A* 81: 022510.

Buchleitner, A., Gremaud, B. & Delande, D. (1994). Wavefunctions of atomic resonances, *Journal of Physics B: Atomic, Molecular and Optical Physics* 27: 2663–2679.

Cao, Y. C. (2011). Impurities enhance semiconductor nanocrystal performance, *Science* 332: 48–49.

Chakraborty, S. & Ho, Y. K. (2011). Autoionization resonance states of two-electron atomic systems with finite spherical confinement, *Physical Review A* 84: 032515.

Chuu, D. S., Hsiao, C. M. & Mei, W. N. (1992). Hydrogenic impurity states in quantum dots and quantum wires, *Physical Review B* 46: 3898–3905.

Ciurla, M., Adamowski, J., Szafran, B. & Bednarek, S. (2002). Modelling of confinement potentials in quantum dots, *Physica E: Low-dimensional Systems and Nanostructures* 15: 261 – 268.

Collins, L. A., S, M., Kress, J. D., Schneider, B. I. & Feder, D. L. (2004). Time-dependent simulations of large-scale quantum dynamics, *Physica Scripta* T110: 408–412.

Connerade, J. P., Dolmatov, V. K., Lakshmi, P. A. & Manson, S. T. (1999). Electron structure of endohedrally confined atoms: atomic hydrogen in an attractive shell, *Journal of Physics B: Atomic, Molecular and Optical Physics* 32: L239–L245.

Cooper, J. W. (1962). Photoionization from outer atomic subshells. a model study, *Physical Review* 128: 681–693.

Costa, L. S., Prudente, F. V., Acioli, P. H., Neto, J. J. S. & Vianna, J. D. M. (1999). A study of confined quantum systems using the Woods-Saxon potential, *Journal of Physics B: Atomic, Molecular and Optical Physics* 32: 2461–2470.

Şahin, M. (2008). Photoionization cross section and intersublevel transitions in a one- and two-electron spherical quantum dot with a hydrogenic impurity, *Physical Review B* 77: 045317.

de Groot, S. R. & ten Seldam, C. A. (1946). On the energy levels of a model of the compressed hydrogen atom, *Physica* 12: 669–682.

Dolmatov, V. K., Baltenkov, A. S., Connerade, J. P. & Manson, S. T. (2004). Structure and photoionization of confined atoms, *Radiation Physics and Chemistry* 70: 417–433.

Ham, H. & Spector, H. N. (n.d.). Photoionization cross section of hydrogenic impurities in spherical quantum dots.

Ho, Y. K. (1983). The method of complex coordinate rotation and its applications to atomic collision processes, *Physics Reports* 99: 1 – 68.

Huang, Y.-S., Yang, C.-C. & Liaw, S.-S. (1999). Relativistic solution of hydrogen in a spherical cavity, *Physical Review A* 60: 85–90.

Kimani, P., Jones, P. & Winkler, P. (2008). Correlation studies in weakly confining quantum dot potentials, *International Journal of Quantum Chemistry* 108: 2763–2769.

Lin, C. Y. & Ho, Y. K. (2011). Photoionization cross sections of hydrogen impurities in spherical quantum dots using the finite-element discrete-variable representation, *Physical Review A* 84: 203407.

Marr, G. V. & Creek, D. M. (1968). The photoionization absorption continua for alkali metal vapours, *Proceedings of the Royal Society A* 304: 233–244.

Michalet, X., Pinaud, F. F., Bentolila, L. A., Tsay, J. M., Doose, S., Li, J. J., Sundaresan, G., Wu, A. M., Gambhir, S. S. & Weiss, S. (2005). Quantum dots for live cells, in vivo imaging, and diagnostics, *Science* 307: 538–544.

Michels, A., de Boer, J. & Bijl, A. (1937). Remarks concerning molecular interactions and their influence of the polarizability, *Physica* 4: 981–994.

Michels, H. H. (1963). Abscissas and weight coefficients for Lobatto quadrature, *Mathematics of Computation* 17: 237–244.

Peach, G., Saraph, H. E. & Seaton, M. J. (1988). Atomic data for opacity calculations. ix. the lithium isoelectronic sequence, *Journal of Physics B: Atomic, Molecular and Optical Physics* 21: 3669–3683.

Ralchenko, Y., Kramida, A. E., Reader, J. & Team, N. A. (2011). *NIST Atomic Spectra Database (ver. 4.1.0)* .
URL: *http://physics.nist.gov/asd3*

Reinhardt, W. P. (1982). Complex coordinates in the theory of atomic and molecular structure and dynamics, *Annual Review of Physical Chemistry* 33: 223–255.

Rescigno, T. N. & McCurdy, C. W. (2000). Numerical grid methods for quantum-mechanical scattering problems, *Physical Review A* 62: 032706.

Rescigno, T. N. & McKoy, V. (1975). Rigorous method for computing photoabsorption cross sections from a basis-set expansion, *Physical Review A* 12: 522–525.

Sahoo, S. & Ho, Y. K. (2006). Photoionization of Li and Na in Debye plasma environments, *Physics of Plasmas* 13: 063301.

Schedelbeck, G., Wegscheider, W., Bichler, M. & Abstreiter, G. (1997). Coupled quantum dots fabricated by cleaved edge overgrowth: From artificial atoms to molecules, *Science* 278: 1792–1795.

Schweizer, W., Faßbinder, P. & González-Férez, R. (1999). Model potentials for alkali metal atoms and Li-like ions, *Atomic Data and Nuclear Data Tables* 72: 33–55.

Stevanović, L. (2010). Oscillator strengths of the transitions in a spherically confined hydrogen atom, *Journal of Physics B: Atomic, Molecular and Optical Physics* 43: 165002.

Winkler, P. (2004). Electron interaction in weakly confining quantum dot potentials, *International Journal of Quantum Chemistry* 100: 1122–1130.

Xie, W. (2009). A study of two confined electrons using the Woods-Saxon potential, *Journal of Physics: Condensed Matter* 21: 115802.

Yang, C.-C., Liu, L.-C. & Chang, S.-H. (1998). Eigenstates and fine structure of a hydrogenic impurity in a spherical quantum dot, *Physical Review B* 58: 1954–1961.

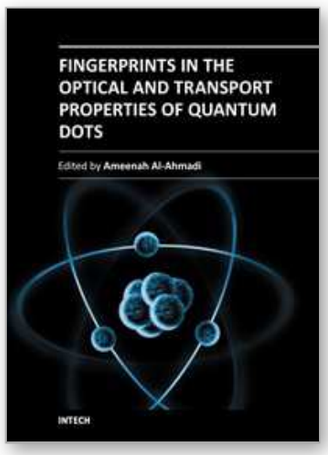

Fingerprints in the Optical and Transport Properties of Quantum Dots

Edited by Dr. Ameenah Al-Ahmadi

ISBN 978-953-51-0648-7
Hard cover, 468 pages
Publisher InTech
Published online 13, June, 2012
Published in print edition June, 2012

The book "Fingerprints in the optical and transport properties of quantum dots" provides novel and efficient methods for the calculation and investigating of the optical and transport properties of quantum dot systems. This book is divided into two sections. In section 1 includes ten chapters where novel optical properties are discussed. In section 2 involve eight chapters that investigate and model the most important effects of transport and electronics properties of quantum dot systems This is a collaborative book sharing and providing fundamental research such as the one conducted in Physics, Chemistry, Material Science, with a base text that could serve as a reference in research by presenting up-to-date research work on the field of quantum dot systems.

How to reference

In order to correctly reference this scholarly work, feel free to copy and paste the following:

C.Y. Lin and Y.K. Ho (2012). Photoionization Cross Sections of Atomic Impurities in Spherical Quantum Dots, Fingerprints in the Optical and Transport Properties of Quantum Dots, Dr. Ameenah Al-Ahmadi (Ed.), ISBN: 978-953-51-0648-7, InTech, Available from: http://www.intechopen.com/books/fingerprints-in-the-optical-and-transport-properties-of-quantum-dots/photoionization-cross-sections-of-atomic-impurities-in-spherical-quantum-dots

INTECH
open science | open minds

InTech Europe
University Campus STeP Ri
Slavka Krautzeka 83/A
51000 Rijeka, Croatia
Phone: +385 (51) 770 447
Fax: +385 (51) 686 166
www.intechopen.com

InTech China
Unit 405, Office Block, Hotel Equatorial Shanghai
No.65, Yan An Road (West), Shanghai, 200040, China
中国上海市延安西路65号上海国际贵都大饭店办公楼405单元
Phone: +86-21-62489820
Fax: +86-21-62489821

© 2012 The Author(s). Licensee IntechOpen. This is an open access article distributed under the terms of the Creative Commons Attribution 3.0 License, which permits unrestricted use, distribution, and reproduction in any medium, provided the original work is properly cited.

IntechOpen

IntechOpen